-RESEARCH PAPER-

International Journal of Mining and Geo-Engineering

IJMGE

IJMGE 57-1 (2023) 73-87

DOI: 10.22059/IJMGE.2022.346697.594987

Coupled effect of tire-derived aggregate and geogrid on lateral earth pressure on high-filled cut-and-cover tunnels

Shamil Ahmed Flamarz Arkawazi [a, b *], Mohammad Hajiazizi [b]

[a] *Civil Engineering Department, Faculty of Engineering, Razi University, Kermanshah City, Kermanshah Province, Iran.*

[b] *Civil Engineering Department, University of Garmian, Kalar City, Sulaimaniya Province, Iraq*

Article History:

Received: 03 August 2022.

Revised: 20 September 2022.

Accepted: 22 October 2022.

ABSTRACT

For the possibility of using valuable lands with plateaus terrain, the High-filled cut-and-cover tunnels (HFCCTs) are considered a practical and successful solution. The HFCCT is first constructed and then backfilled in layers in the trench, which is different from traditional tunnel construction methods. Because the high amount of backfill soil above the HFCCT produces ultrahigh earth pressure, it is necessary to use load reduction methods to reduce the earth pressure on the HFCCT, which will reduce the tunnel designing structure loads and increase safety. This study describes two load reduction methods using a combination of tire-derived aggregate (TDA) and geogrid. Abaqus CAE 2019 software, based on the finite element method, was employed to analyze and examine the lateral earth pressure (LEP) reduction progress and mechanism. Several influential factors, including the geogrid presence effect, the TDA form, the TDA thickness, and the distance between the top of the HFCCT and the bottom of the TDA were studied. The analysis results focused on changes in average LEP, relative vertical displacement of the HFCCT backfill soil prisms, and the effect of geogrid presence on the top of the TDA. This study found that the factors are influential and have significant effects on the average LEP reduction on the HFCCT through the load reduction mechanisms, which include relative vertical displacements of the HFCCT backfill soil prisms and soil arching, where the average LEP on the top of the HFCCT model reduced from 303 kPa to 125 kPa (58.745% reduction in the average LEP).

Keywords: *Geogrid; High-filled cut-and-cover tunnels; Lateral earth pressure; Tire-derived aggregate.*

1. Introduction

The high-filled cut-and-cover tunnels (HFCCTs) provide a specific solution for the possibility of using valuable lands with mountainous or hills terrain around the world. The primary property of the various HFCCTs is their high or extra-high backfill soil. However, the ultrahigh earth pressure developed or induced on the top or side of the cut-and-cover tunnel (CCT) can cause structural problems and safety concerns. Research and studies concerning the load reduction effect in the backfill soil above culverts and pipes have been conducted since the early years of the 20th century; but, a limited number of researches focused on and studied HFCCTs-related issues, especially what is related to load and load reduction on the HFCCTs.

Marston initiated the concept of 'induced trench installation' for rigid pipes buried under high embankment fill. Loads on buried rigid pipes and conduits are usually determined based on Marston's theory [1].

In 1922 Marston confirmed that the major factor which affects the earth pressure on underground conduits is dependent on the relative settlement between the soil column (interior prism) immediately above the culvert and the adjacent soils (exterior prisms) that govern the magnitude and direction of friction, thus affecting the earth pressure on the culvert structure. A compressible material zone, such as leaves, baled straw, woodchips or sawdust, and expanded polystyrene (EPS) geofoam, can be placed above culverts to reduce the earth pressure on the culverts and induce positive soil arching [2-10].

The HFCCTs are common in northwestern China because the HFCCTs construction allows reclaiming of usable land over the CCT. However, because of the unique land terrains of the Loess Plateau in this region of China, the backfill soil quantity required for HFCCTs is enormous, and the backfill must be sufficiently high to maximize the valuable, usable land. The major challenge of HFCCTs construction is high earth pressure and safety concerns related to the existing CCT lining structure [11].

A study was conducted to discuss the physical modeling tests conducted to investigate: load reduction methods that use expanded polystyrene (EPS) in the backfill soil; and structural modifications to the CCTs. The results of the experiments agree well with the results of the numerical analysis. The numerical analysis was used to determine suitable EPS thicknesses for load reduction on the CCT when subjected to different backfill heights. The internal forces could be changed by modifying the cross-sectional shape of the lining structure of the CCT to make the concrete of the CCT structure support more compressive loads instead of yielding to bending moments. The study results showed that the coupled effects of load reduction using EPS and cross-sectional modifications of the CCT lining structure could significantly reduce the required thickness of the CCT lining structure, increase the allowable backfill height and enhance the safety of the CCT [11].

A study was conducted to describe a study of three load reduction measures: expanded polystyrene (EPS); a combination of EPS and geogrid; and a combination of EPS, geogrid, and concrete wedges. A computer program based on the discrete element method (DEM) called PFC2D was employed to examine and analyze the load reduction

* Corresponding author. Tel/Fax: +9647701244450, *E-mail address:* shamil.flamarz@garmian.edu.krd (S. A Flamarz Arkawazi).

mechanisms' evolution. Parametric studies were conducted to check and investigate six significant and influential factors: the thickness, density, and width of the EPS, the level or location where the EPS was placed in the structure, the number of layers of the geogrid, and the tensile strength of the geogrid. The analysis results were based on the observed changes in average vertical earth pressure (VEP), relative vertical displacement of the backfill soil, the contact force among backfill soil particles, and relative vertical deformation of the geogrid. The research determined that these influential factors have significant or considerable effects on the soil arching effect and the tensioned member effect in the load reduction mechanisms. For optimizing load reduction of the earth pressure on the top of HFCCTs, the influential factors' optimum values were derived [12].

HFCCTs can assist in satisfying the enormous demand for valuable, usable lands. However, this reclamation tunneling construction method involves massive backfill over a CCT, which produces high pressure on the tunnel. A better understanding of load reduction mechanisms that can reduce this load could also help to improve safety and reduce design costs. The load on top of CCTs can be reduced using relatively low compacted (RLC) soil; however, using the RLC soil layer in the load reduction on the top of CCTs makes the load transfer mechanisms more complex. Previous studies have either focused mainly on the micromechanical properties of soils or ignored their distinct properties. Thus, if the soil's micromechanical properties can be appropriately considered, then the mechanisms of load transfer can be understood in a better way. Backfill the CCTs with different relative compaction (R) percentages should be considered: e.g., *R*=90% for major backfill soil and *R*=80% for the RLC layer placed over the HFCCT [9].

RLC soil can reduce the ultrahigh loads on the HFCCTs in the short term, but it is unknown the ability of the RLC soil to reduce the load on the HFCCTs in the long term. In the HFCCT design, the soil arching effect resulting from soil creep must be carefully considered. A study consists of three stages of analysis conducted: during backfilling creep, immediately (0 months) after backfilling, and after the deformation of soil is finished (20 years). FLAC3D, a finite element software, was employed to investigate the VEP and the vertical displacement of the backfill soil around the HFCCT. The Burgers model was used for the simulation of the creep behavior of soil. Furthermore, parametric studies were conducted for different locations and dimensions of RLC soil. The results showed that the soil arching effect resulting from the RLC soil inclusion performs well initially in reducing the load but lately disappears, which can produce a significant load rebound of more than 100 kPa and endanger the stability of the HFCCT [13].

The discrete element method (DEM) software was used to investigate the changes in VEP on HFCCTs relative to the spread distance and thickness of the RLC soil layer, the valley width to the width of the CCT ratio (the B/D ratio), and the slope angle. To characterize these influential factors, parametric DEM studies were conducted. The results of the DEM study showed that a proper thickness and spread distance of the RLC soil layer could optimize the effect of soil arching and reduce VEP on top of CCTs. The results also showed that the slope angle and B/D ratio are relevant to the reorientation of the VEP [9].

Due to the high amount of backfill soil, ultrahigh earth pressure generated on the HFCCT structure can affect the safety of the HFCCT. For earth pressure reduction on the HFCCT, the DEM was used to introduce three load reduction methods: the HFCCT cross-section type, the combination of HFCCT optimized cross-section type and with load reduction using EPS, and the combination of HFCCT optimized cross-section type with load reduction using the EPS and the concrete wedge. The changes in earth pressure on the HFCCTs were evaluated concerning the EPS density, the position of EPS, and the height and width of the concrete wedge. DEM parametric studies were conducted to describe these influential factors. It was found from the results of the study that different cross sections of HFCCT have different influences on earth pressure distribution, and the effects of EPS on load reduction were very clear, resulting in a significant reduction in VEP on top of HFCCT and a small increase in LEP on the sides of HFCCT. In addition, concrete wedges installation reduced the VEP and LEP of HFCCT. These factors showed significant effects on the load reduction mechanisms of HFCCT. Based on the influences of these factors on the earth pressure of HFCCT from a microscopic view, optimum values for the influential factors were determined [14].

A case was reported in which tire-derived aggregate (TDA) was applied successfully to reduce the backfill weight on a cut-and-cover railway tunnel. 3D numerical analyses were used to determine the effect of different assumptions about the TDA constitutive model. Also, other formations of TDA around the CCT section were examined. Up to 60%, reductions inlining bending moment can be achieved. For the case analyzed, the elastic property of the TDA has little influence on CCT lining loads, although it is essential for backfill settlement estimates [9].

The soil arching effect also can be derived from using EPS or from the coupling effect of using EPS and geogrid to reduce the overload of earth pressure on HFCCTs. For this purpose, a study was conducted to investigate the load transfer mechanisms affected by the placement of EPS and geogrid over an HFCCT using the discrete element method (DEM) [15].

This study presents a numerical investigation of the coupled effect of using TDA as a compressible material and geogrid in two different forms on LEP reduction on HFCCTs. The research includes using tire-derived aggregate (TDA) and geogrid in horizontal and combined horizontal and arch forms above the HFCCT structure with six thicknesses; 0.5 m, 1.0 m, 1.5 m, 2.0 m, 2.5 m, and 3.0 m and three distances between the bottom of the TDA and top of the HFCCT; 0.25 m, 0.5 m, and 1.0m. Several influential factors, including the geogrid presence effect, the TDA form, the TDA thickness, and the distance between the bottom of the TDA and the top of the HFCCT, will be studied. The analysis results will focus on changes in average LEP, relative vertical displacement of the HFCCT backfill soil prisms, and the effect of geogrid presence on the top of the TDA.

2. The high-filled cut-and-cover tunnel (HFCCT) study model

Figure 1 shows the cross-section of the HFCCT study model, where a 4-lane road CCT is located at the base of a valley with 50 m vertical depth, 23.4 m base width, and approximately 70^0 angles of side slopes. The backfill height of the CCT is 42.3 m, and the height and width of the CCT were designed to be 7.7 m and 15.4 m, respectively.

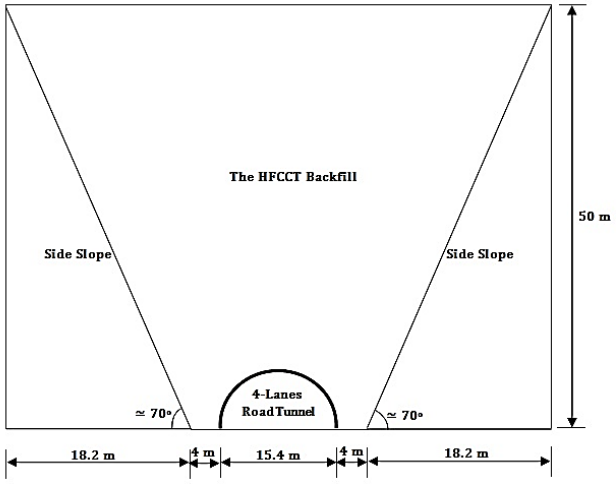

Figure 1: The high-filled cut-and-cover tunnel (HFCCT) study model

3. Material parameters

3.1. Backfill soil parameters

The physical and mechanical properties of the backfill soil were determined by conducting the relevant laboratory tests. The cohesion, c, the internal friction angle, φ, and Young's modulus value were

determined by performing triaxial compression tests. A standard test following ASTM D4253-00 [16] was used to obtain other properties, such as optimal moisture content and maximum dry density. The backfill soil test results are shown in Table 1.

3.2. Tire-derived aggregate (TDA) parameters

The American Society for Testing and Materials (ASTM) in ASTM D6270-08, "Standard Practice for Use of Scrap Tires in Civil Engineering Applications", provided a comprehensive and detailed list of terms and definitions and outlined the standard practice for scrap tires used in civil engineering applications [17].

TDA has been used as an alternative embankment filling material because of its lightweight. TDA is one-third of the conventional fill material weight and therefore produces less pressure on the underlying material. This can be an advantage and beneficial when designing an embankment fill project in which the underlying foundation soil cannot support the high weight of a conventional soil backfill. In addition to that, TDA has high permeability and, therefore, mainly does not require the placement of sub-drain systems. This will provide additional savings in the cost. TDA as a lightweight fill material has proven to be a cost-effective alternative to other materials such as geofoam and pumice. There are other benefits of TDA in an embankment and road fill and applications like reinforcing roadway shoulders, increasing the stability of steep slopes along roadways, and providing an insulating layer against frost penetration due to its thermal resistance properties. The ASTM standard divided TDA into two major types used in engineering applications, Type A and Type B, and two fill classes associated with them, Class I and Class II. Type A and Type B are TDA size classifications used for different engineering applications. Class I and Class II describe the fill lift thicknesses as defined by ASTM D6270-08, Section 6.10.1. Type A material is roughly 75 to 100 mm in size, and Type B material is approximately 152.4 to 304.8 mm. Class I fills are TDA layers that are less than 1 meter in height, and Class II fills describe TDA layers that are between 1 and 3 meters high. Typically Type A material is used in Class I fills, and Type B material is used in applications requiring a Class II fill. Table 2 summarizes Type A, and Type B size classifications and Figure 2 shows photos of typical samples of TDA material. Because TDA is a compressible material, the density of TDA varies depending on whether it is being stockpiled or installed in the project. The stockpile and shipping densities of Type A and B TDA range from 400.461 to 560.646 kg/m^3, while compacted in-place density values for Type A and B TDA ranges from approximately 560.646 to 800.923 kg/m^3 (see Table 3) [18].

Modulus of elasticity (E) is the coefficient of proportionality between the applied stress and the measured strain; for example, in a one-dimensional tensile test, the lower values of E are indicative of layer deformation. The elastic modulus (E) for TDA ranges from 1.241 MPa to 5.171 MPa [17]. For comparison purposes, the elastic modulus (E) of dense, drained sands can vary from 41.368 MPa to 82.737 MPa [19]. The modulus of elasticity (E) for gravel is much larger. Therefore, under the same stress conditions, the TDA will deform much more than the soil. Poisson's ratio (ν) is the ratio of transverse strain to longitudinal strain, as measured for example, in a one-dimension tensile test, the Poisson's ratio of TDA is 0.5 [17], which means that the TDA material would deform at a constant volume. As a comparison, the Poisson's ratio (ν) for mineral aggregate varies from 0.15 to 0.45 [19].

For numerical analysis, the required TDA material engineering properties were selected and summarized in Table 4.

3.3. Geogrid

Geogrids usually are made of polymeric materials such as high-density polyethylene, polyester, and polypropylene. The manufacturing of geogrid includes a different process (extruded and punched-drawn, welding, or knitting) [20]. They are manufactured by the extruded and punched-drawn have rigid joints at nodes and are unitized, and the angle between two adjacent ribs does not change during loading due to much larger thickness at nodes than ribs. The geogrids were manufactured with apertures in a square or rectangular shape and were used to carry tensile forces in one or two directions along the ribs. The one-directional tensile strength geogrid is known as a uniaxial geogrid and is used for slopes and walls [21]. The two-directional tensile strengths geogrid is named bidirectional or biaxial geogrid and is used for pile-supported embankments, roads, and foundations. Geogrid's uses have been increasing over the past 30 years, and it is expected to keep expanding and rising. About ten years ago, the geogrid with a triangular aperture was introduced into the market. The triangular aperture geogrid is manufactured with three equilateral directions oriented ribs and is expected to have a more stable grid structure and provide more uniform resistance to tensile forces in all directions, and is expected the geogrid with triangular apertures to be used in similar applications as bidirectional (biaxial) geogrid especially when the loading is not only in two directions [22]. Figure 3 shows the rectangular and triangular apertures geogrid.

The uses of bidirectional geogrids for foundation reinforcement, sub-grade improvement, pile-supported embankments, and base and ballast reinforcement studied by many researchers [23-30]. Table 5 includes some of the studies conducted using different types of geogrids with their properties, and Figure 4 shows the typical geogrids with rectangular and triangular apertures. For numerical analysis, the required geogrid properties were selected and summarized in Table 6.

4. Numerical analysis and model creation

All the numerical analysis works in this study were conducted using Complete Abaqus Environment 2019 (Abaqus CAE 2019), which is based on the finite element method. For the numerical analysis works, a finite element model was created with a 1/50 scale of the actual HFCCT study model (see Figure 5). In the finite element model, the slopes are assumed to be rigid. Abaqus CAE Standard/Explicit Model, which uses plane strain element type, is selected to model the HFCCT. The boundaries at two sides of the finite element model are restrained in horizontal directions using rollers so that only vertical displacement is allowed, and the bottom boundary of the model is entirely fixed. The Mohr-Coulomb elastoplastic criterion was used to model the backfill soil and TDA material. The linear elastic, isotropic criterion was used to model the geogrid. Then the geogrid section was created using a homogeneous shell section. The shell thickness and associated material were then specified, as for the element type, the S4R (a four-node doubly curved thin or thick shell, reduced integration, hourglass control, finite membrane strains) element type was selected. S4R is a robust, general-purpose element suitable for a wide range of applications. For accurate numerical analysis results, mesh size and orientation sensitivity tests were investigated. The parameters used in the finite element analysis, such as the mechanical properties for backfill soil, TDA, and geogrid, are summarized in Table 7.

Table 2: TDA fill classes (ASTM D6270-08 Section 6.10.1-4) [18].

Characteristics	TDA Type A	TDA Type B
Fill Class	Class I	Class II
Typical Size	75-100 mm	150-300 mm
Maximum Layer Depth	Less than 1 m	Less than 3 m

Table 3: Densities of type A and type B tire-derived aggregate (TDA) [18].

Stages	TDA Type A, Kg/m^3	TDA Type B, Kg/m^3
Shipping and Stockpiling	400.461-560.646	400.461-560.646
Compacted	720.830-848.978	720.830-800.923

Table 1: Engineering properties of backfill soil.

Cohesion (c) (KPa)	Internal friction angle (φ) (°)	Young's modulus (E) (MPa)	Poisson's ratio (ν)	Optimum moisture content (W_{opt}) (%)	Maximum dry density (ρ_d) (Kg/m^3)	Saturated density (ρ) (Kg/m^3)
7.2	36	11.250	0.3	25.1	1690	1870

Table 4: Engineering properties of TDA material [16, 18].

The density of TDA ρ (kg/m3)	Cohesion C (kPa)	The angle of internal friction φ (°)	Modulus of elasticity E (kPa)	Poisson's ratio υ
400.461	10	23	630	0.2

Figure 2: Up - Type A tire-derived aggregate (TDA),
Down - Type B tire-derived aggregate (TDA) [18].

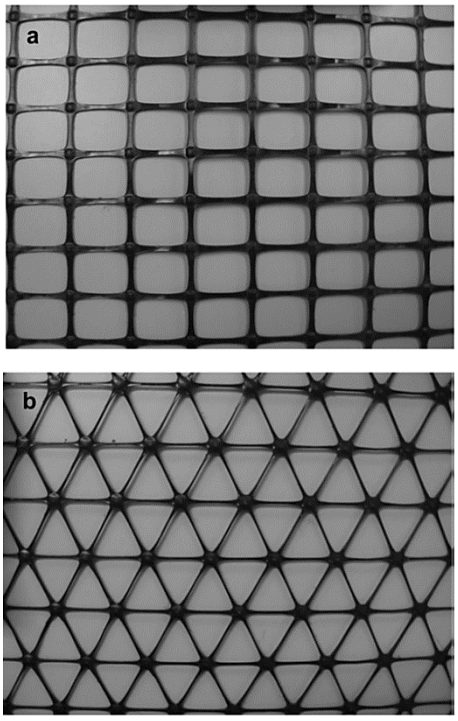

Figure 3: Rectangular and triangular apertures geogrid products (extruded and punched-drawn)
(a) Rectangular apertures geogrid, (b) Triangular apertures geogrid [22]

5. Results of numerical analysis

5.1. LEP estimation on the HFCCT for the base conditions of the study model (no-load reduction method is used)

A numerical analysis was conducted to estimate the average lateral earth pressure (LEP) on the finite element HFCCT study model with the base conditions (no-load reduction method used) (see Figure 6). The average LEP on the top of the actual HFCCT study model with the base conditions was estimated based on the average LEP estimation on the finite element HFCCT study model, and its value is 303 kPa.

5.2. LEP estimation on the HFCCT for the study model with load reduction method using TDA and geogrid in a horizontal form

Figures 7 and 8 present the relationships of the average LEP and the percentage of reduction in the LEP on the top of the HFCCT study model with the TDA thickness (TDA is in a horizontal form with the presence of geogrid on the top of the TDA) and the distance between the top of the HFCCT and the bottom of the TDA. For all the TDA thicknesses (0.5 m, 1.0 m. 1.5 m, 2.0 m, 2.5 m, and 3.0) and the distances between the top of the HFCCT and the bottom of TDA (0.25 m, 0.5 m and 1.0 m), the average LEP on the top of the HFCCT study model reduces from 303 kPa to 125 kPa (58.745% reduction in the average LEP on the top of the HFCCT study model), which can be considered good result in term of average LEP reduction on the top of the HFCCT, in addition to this method of load reduction is good in terms of average LEP reduction on the top of the HFCCT, it indicated that increasing the TDA thickness and the distance between the top of the HFCCT and the bottom of TDA will not have any influence in term of average LEP reduction on the top of the HFCCT, although increasing the TDA thickness and the distance between the top of the HFCCT and the bottom of TDA in this method of load reduction will not have any influence on the average LEP on the top of the HFCCT, they will have a considerable effect on the average LEP values in the other parts of the backfill of the HFCCT study model (see Figures 9, 10 and 11). It is significant to reduce the LEP on the HFCCT, but not to a limit that causes a negative influence because LEP can help and work on stabilizing the structure of the HFCCT.

The TDA inclusion in a horizontal form with the presence of geogrid on top of the TDA leads the soil prism (interior prism) within the HFCCT structure width to settle more than the surrounding soil prisms (exterior prisms) in a uniform and equal level due to deformation of the TDA and geogrid control of the TDA settlement and keep it in equal and uniform level (see Figures 12, 13, 14, 15 and 16), the soil prism (interior prism) within the HFCCT structure width deform in equal and uniform level. Meanwhile, the reduced VEP on the HFCCT structure is equal to the magnitude of the shear force on the soil in the interior prism. The VEP reduction will lead the LEP to be reduced as the LEP value mainly depends on γh (h: the height of backfill above the HCCT and γ: the unit weight of backfill material above the HCCT).

It is worth mentioning that the light gray color at the top of the interior prism in the backfill of the HFCCT in the contours of average LEP on the HFCCT with TDA inclusion in a horizontal form with the presence of geogrid on top of the TDA refers to tensile forces resulting from the soil prism (interior prism) within the HFCCT structure width settle more than the surrounding soil prisms (exterior prisms) of the HFCCT backfill (see Figures 9, 10 and 11).

Table 5: Some studies conducted using different types of geogrids with their properties.

No.	Ref.	The research title	Type or brand of the geogrid used in the research	Density (ρ) (kg/m³)	Elastic modulus (E) (GPa)	Poisson's Ratio (ν)	Joint thick. (mm)	Ribs thick. (mm)
1-	[31]	An assessment of the geometry effect of geosynthetics for base course reinforcements	Biaxial geogrid (BX) Triaxial geogrid (TX)		2.63 2.63	0.333 0.333	1.27 1.95	1.27 1.95
2-	[32]	Numerical Modeling and Analysis of Pullout Tests of Sheet and Geogrid Inclusion in Sand	GGT GGS GGM		0.036 0.096 0.096	0.2		
3-	[33]	The Mechanical Property of Bidirectional Geogrid and its Application Research in Retaining Wall Design	Bidirectional geogrid	1900	0.65	0.21		
4-	[34]	Advanced Numerical Modeling of Geogrid-reinforced Rockfall Protection Embankments		0.42 (kg/m²)	0.2	0.3		
5-	[35]	Experimental Investigation of Geogrid Reinforced Concrete Slab	Biaxial geogrid	900	27.750	0.25	4	4
6-	[36]	3D-FEM Analysis on Geogrid Reinforced Flexible Pavement Roads	Glass fiber grid		28	0.3	3	3
7-	[37]	Characterization of Geogrid Reinforced Ballast Behavior Through Finite Element Modeling	G1 G2 G3	600 800 1100	0.007 0.012 0.030	0.300 0.300 0.316	7.5	7.5
8-	[38]	Use of Reinforced Soil Foundation (RSF) to Support Shallow Foundation	- Mirafi BasXgrid11 geogrid - Tensar BX6100 geogrid - Tensar BX6200 geogrid - Tensar BX1100 geogrid - Tensar BX1200 Geogrid - Tensar BX1500 geogrid - Tenax MS330 Geogrid - Mirafi Miragrid 8XT geogrid		0.071568 0.150030 0.300474 0.327087 0.376592 0.629353 0.703955 0.908729	0.3 0.3 0.3 0.3 0.3 0.3 0.3 0.3		
9-	[39]	Three-Dimensional Finite Element Modelling of Soil Arching in Pile-Supported Geogrid-Reinforced Embankments			0.1306	0.2	2	2
10-	[40]	Effects of Geogrid Layers on Improving Bearing Capacity of Vibrating Machines Foundation		1000	0.472	0.3		
11-	[41]	Polymer Geogrids: A Review of Material, Design and Structure Relationships	- Polyethylene Terephthalate (PET) - High-Density Polyethylene (HDPE) - Low-Density Polyethylene (LDPE) - Polypropylene (PP) - Polyvinyl Chloride (PVC)	1380 930–970 910–940 920–985 1400	2.76–4.14 0.65–1.5 0.19–0.52 1.14–1.55 0.003–4.14			
12-	[42]	Measurement of Tensile Properties of Geogrids	- Netlon CE121 geogrid - Tensar SS2 geogrids - properties of Iraqi geogrid - China geogrid - SQ12 geogrids - SQ15 geogrids - CE131 geogrids	0.74 (kg/m²) 0.3 (kg/m²) 0.255 (kg/m²) 0.283 (kg/m²) 0.318 (kg/m²) 0.385 (kg/m²) 0.429 (kg/m²)	0.39 0.57/0.99 0.083 0.03 0.28 0.12/0.54 0.32		2.75 3.9 3.3 1.9 1.6 3.3 5	1.6/1.45 1.2/1.1 1.4/2.25 1.2/1.1 1.7 2 2.8
13-	[22]	Numerical analysis of tensile behavior of geogrids with rectangular and triangular apertures	- Biaxial geogrids MD/XMD	2.625/6.552				1.27

Table 6: Geogrid required properties numerical analysis [23].

The density of geogrid (ρ) (kg/m3)	Modulus of elasticity (E) (MPa)	Poisson's ratio (υ)	Thickness (mm)
900	27750	0.25	4

Table 7: Mechanical properties of materials required for the finite element analysis.

Material	Density (ρ) (Kg/m³)	Unit weight (γ) (kN/m3)	Young's modulus (E) (MPa)	Poisson's ratio (ν)	Cohesion C (kPa)	The angle of internal friction (φ) (°)	Thickness (mm)
Backfill soil	1870	18.70	11.25	0.3	7.2	36	-
TDA	400.461	4.00461	0.63	0.2	10	23	-
Geogrid	900	9	27750	0.25	-	-	4

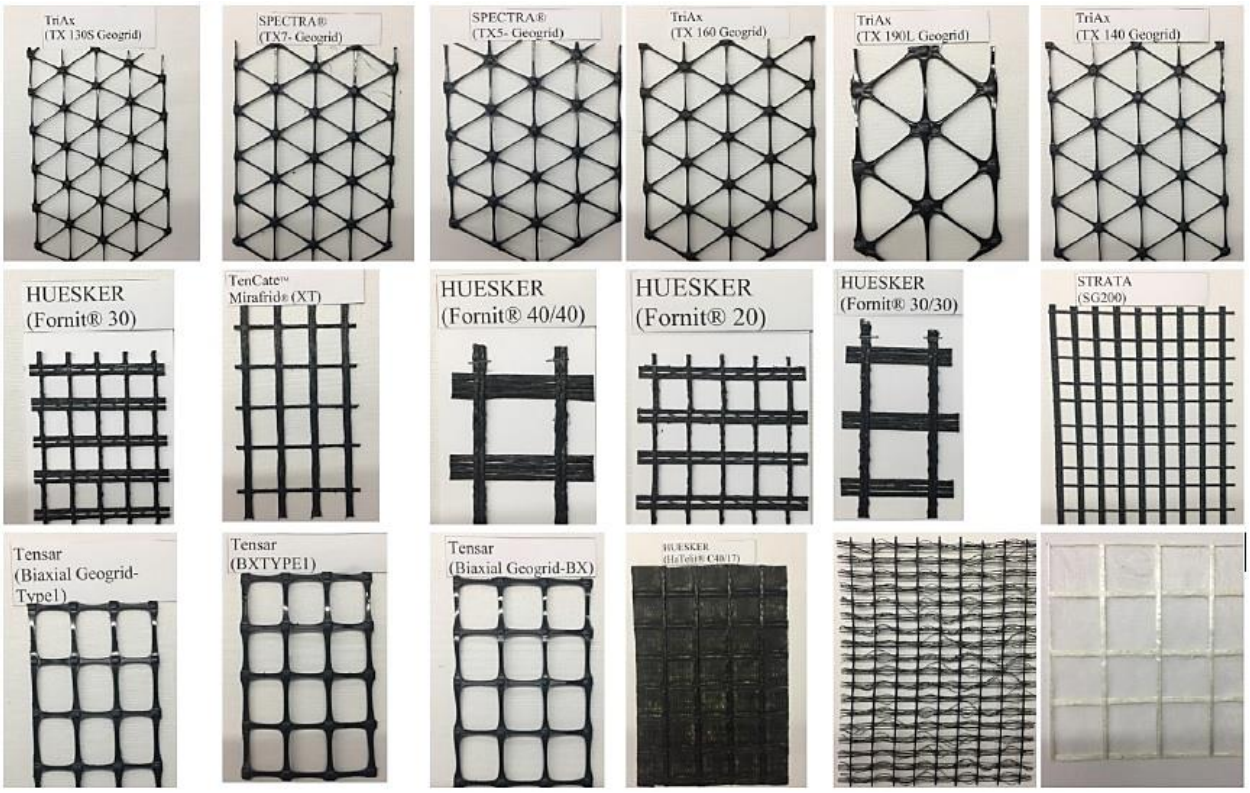

Figure 4: Various types of geogrid with different manufacturing materials [29].

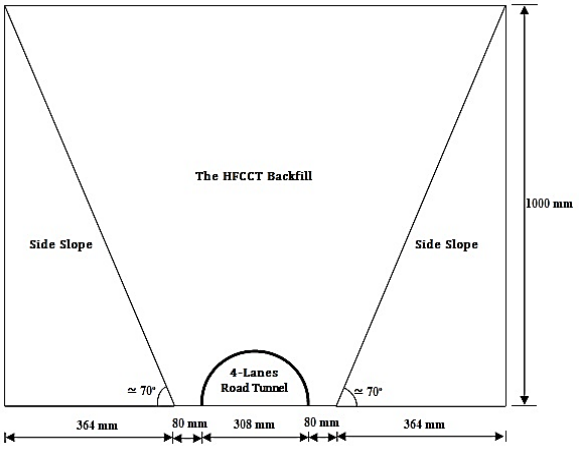

Figure 5: The finite element HFCCT model created with a 1/50 scale of the actual HFCCT study model.

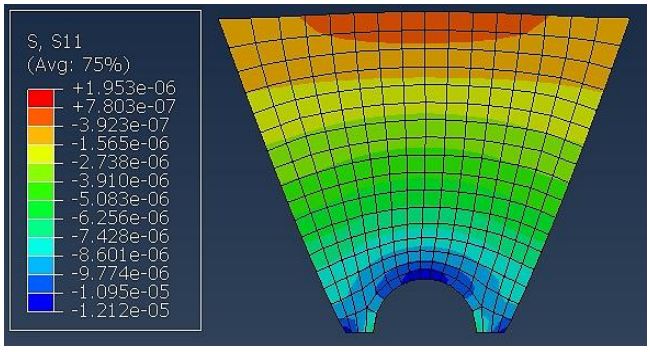

Figure 6: Contours of average lateral earth pressure (LEP) for the base conditions (no-load reduction method used).

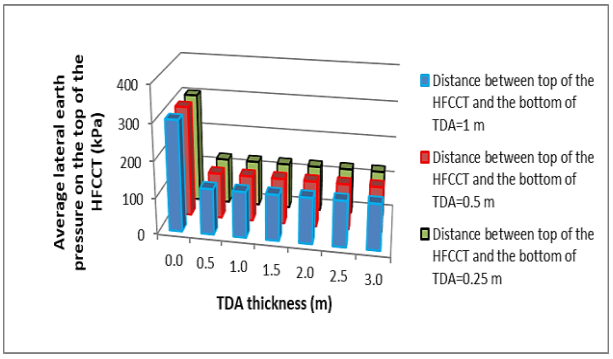

Figure 7: The relationship of the average VEP on top of the HFCCT study model with the TDA thickness (TDA is in a horizontal form with the presence of geogrid on the top of the TDA) and the distance between the top of the HFCCT and the bottom of the TDA.

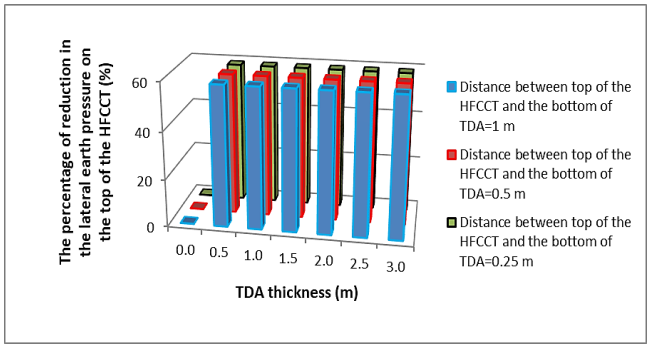

Figure 8: The relationship of the percentage of reduction in the VEP on top of the HFCCT study model with the TDA thickness (TDA is in a horizontal form with the presence of geogrid on the top of the TDA) and the distance between the top of the HFCCT and the bottom of the TDA.

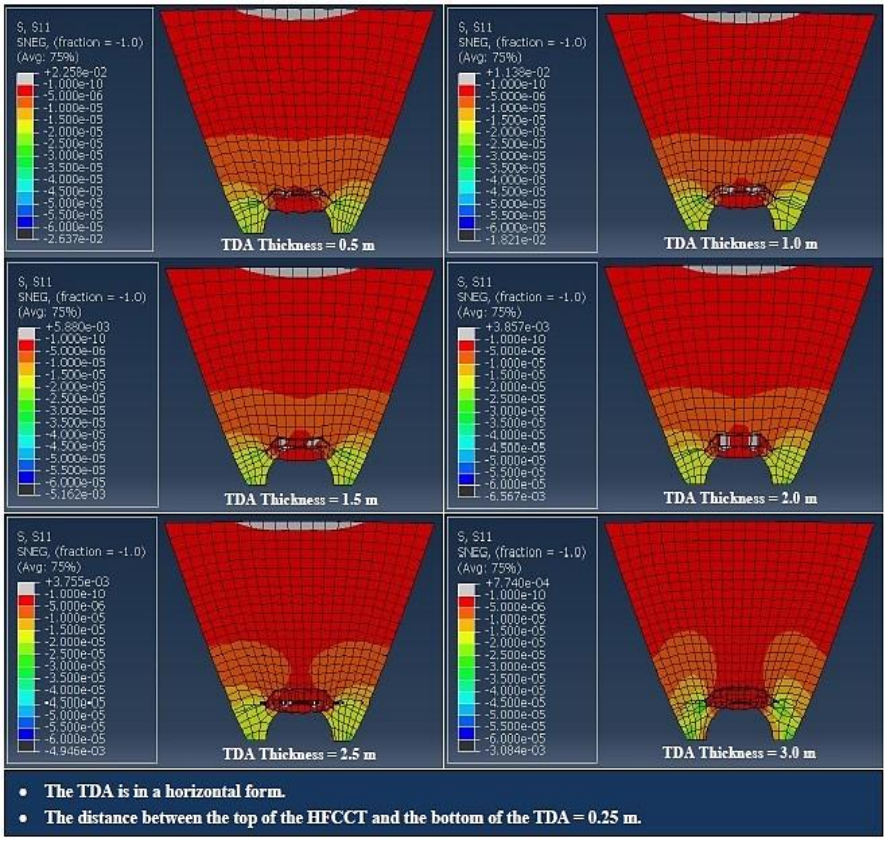

Figure 9: Contours of average LEP for using TDA with the thicknesses of 0.5 m, 1.0 m, 1.5 m, 2.0 m, 2.5 m, and 3.0 m in a horizontal form and the presence of geogrid on the top of the TDA and 0.25 m distance between the top of the HFCCT and the bottom of the TDA (as a method of load reduction on the HFCCT).

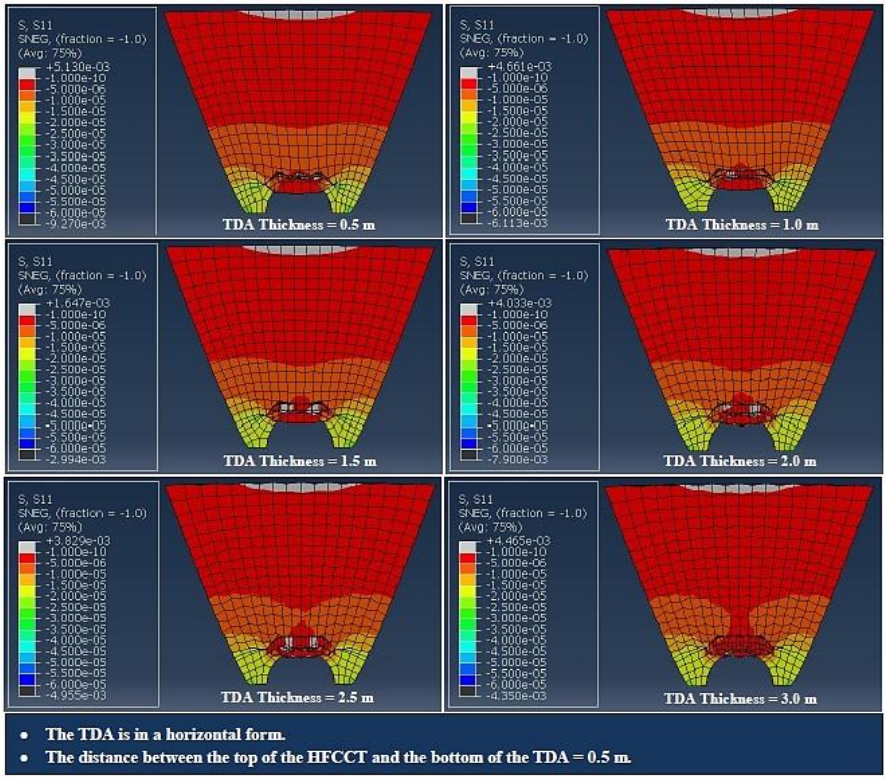

Figure 10: Contours of average LEP for using TDA with the thicknesses of 0.5 m, 1.0 m, 1.5 m, 2.0 m, 2.5 m, and 3.0 m in a horizontal form and the presence of geogrid on the top of the TDA and 0.5 m distance between the top of the HFCCT and the bottom of the TDA (as a method of load reduction on the HFCCT).

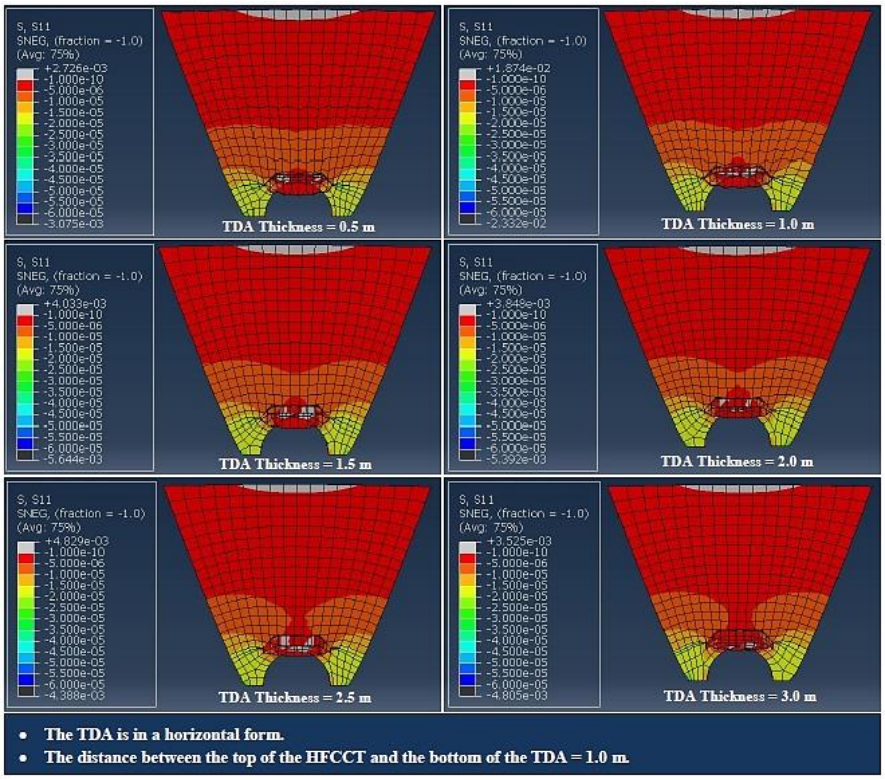

Figure 11: Contours of average LEP for using TDA with the thicknesses of 0.5 m, 1.0 m, 1.5 m, 2.0 m, 2.5 m, and 3.0 m in a horizontal form and the presence of geogrid on the top of the TDA and 1.0 m distance between the top of the HFCCT and the bottom of the TDA (as a method of load reduction on the HFCCT).

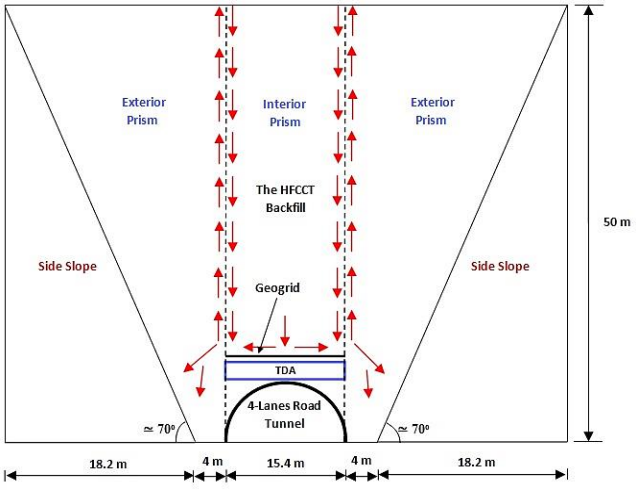

Figure 12: The effect of TDA inclusion in a horizontal form with the presence of geogrid on the top of the TDA on the VEP reduction in the HFCCT study model.

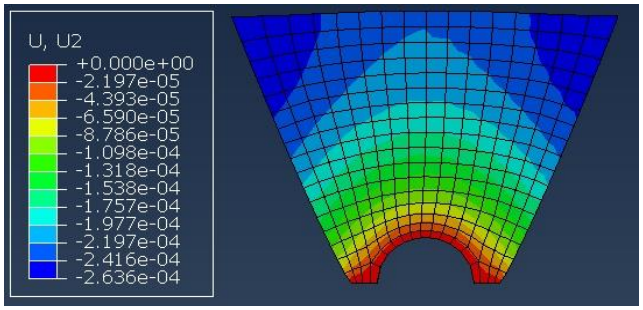

Figure 13: Contours of vertical displacement for the base conditions (no-load reduction method used) of the study model.

5.3. LEP estimation on the HFCCT for the study model with load reduction method using TDA and geogrid in a combined horizontal and arch form

Figures 17 and 18 present the relationships of the average LEP and the percentage of reduction in the LEP on the top of the HFCCT study model with the TDA thickness (TDA is in a combined horizontal and arch form with the presence of geogrid on the top of the TDA) and the distance between the top of the HFCCT and the bottom of the TDA. For all the TDA thicknesses (0.5 m, 1.0 m. 1.5 m, 2.0 m, 2.5 m, and 3.0) and the distances between the top of the HFCCT and the bottom of TDA (0.25 m, 0.5 m and 1.0 m), the average LEP on the top of the HFCCT study model reduces from 303 kPa to 125 kPa (58.745% reduction in the average LEP on the top of the HFCCT study model), which can be considered good result in term of average LEP reduction on the top of the HFCCT, in addition to this method of load reduction is good in terms of average LEP reduction on the top of the HFCCT, it indicated that increasing the TDA thickness and the distance between the top of the HFCCT and the bottom of TDA will not have any influence in term of average LEP reduction on the top of the HFCCT, although increasing the TDA thickness and the distance between the top of the HFCCT and the bottom of TDA in this method of load reduction will not have any influence on the average LEP on the top of the HFCCT, they will have a considerable effect on the average LEP values in the other parts of the backfill of the HFCCT study model (see Figures 19, 20 and 21). It is significant to reduce the LEP on the HFCCT, but not to a limit that causes a negative influence because LEP can help and work on stabilizing the structure of the HFCCT.

The TDA inclusion in a combined horizontal and arch form with the presence of geogrid on top of the TDA leads the soil prism (interior prism) within the HFCCT structure width to settle more than the surrounding soil prisms (exterior prisms) in a uniform and equal level due to deformation of the TDA and geogrid control of the TDA settlement and keep it in equal and uniform level (see Figures 22, 13, 23, 24 and 25), the soil prism (interior prism) within the HFCCT structure

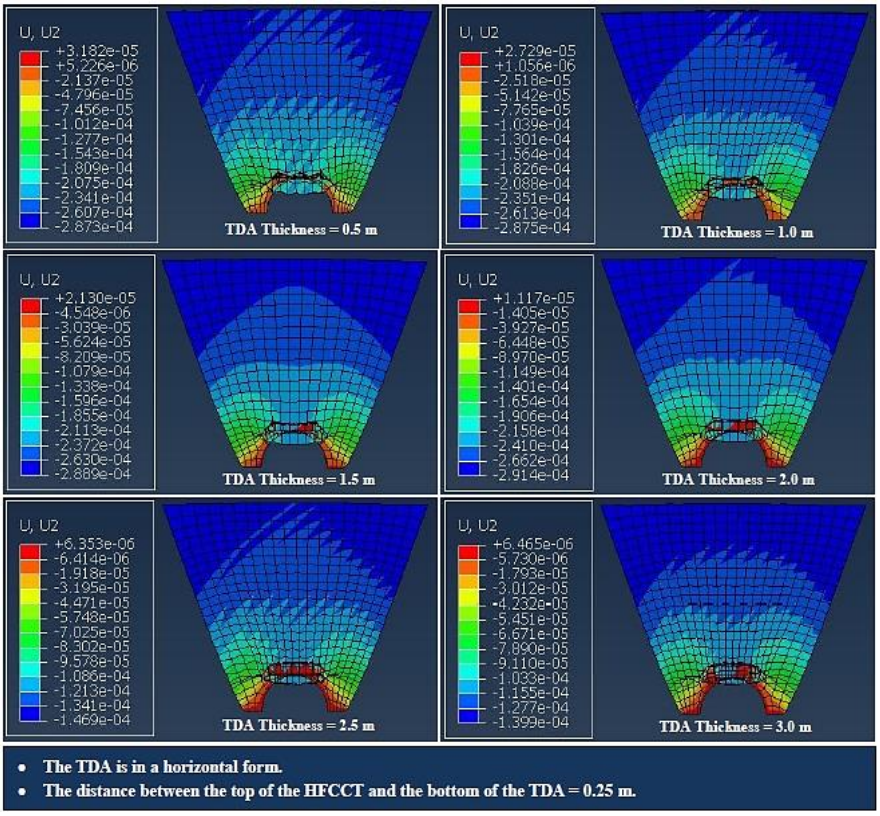

Figure 14: Contours of vertical displacement for using TDA with the thicknesses of 0.5 m, 1.0 m, 1.5 m, 2.0 m, 2.5 m, and 3.0 m in a horizontal form and the presence of geogrid on the top of the TDA and 0.25 m distance between the top of the HFCCT and the bottom of the TDA (as a method of load reduction on the HFCCT).

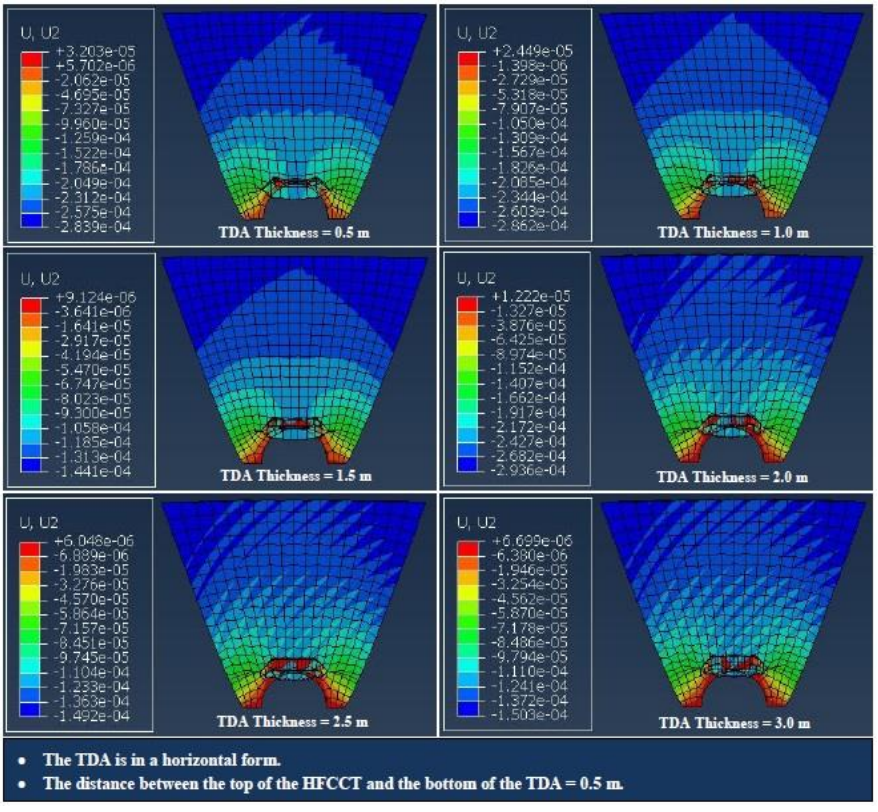

Figure 15: Contours of vertical displacement for using TDA with the thicknesses of 0.5 m, 1.0 m, 1.5 m, 2.0 m, 2.5 m, and 3.0 m in a horizontal form and the presence of geogrid on the top of the TDA and 0.5 m distance between the top of the HFCCT and the bottom of the TDA (as a method of load reduction on the HFCCT).

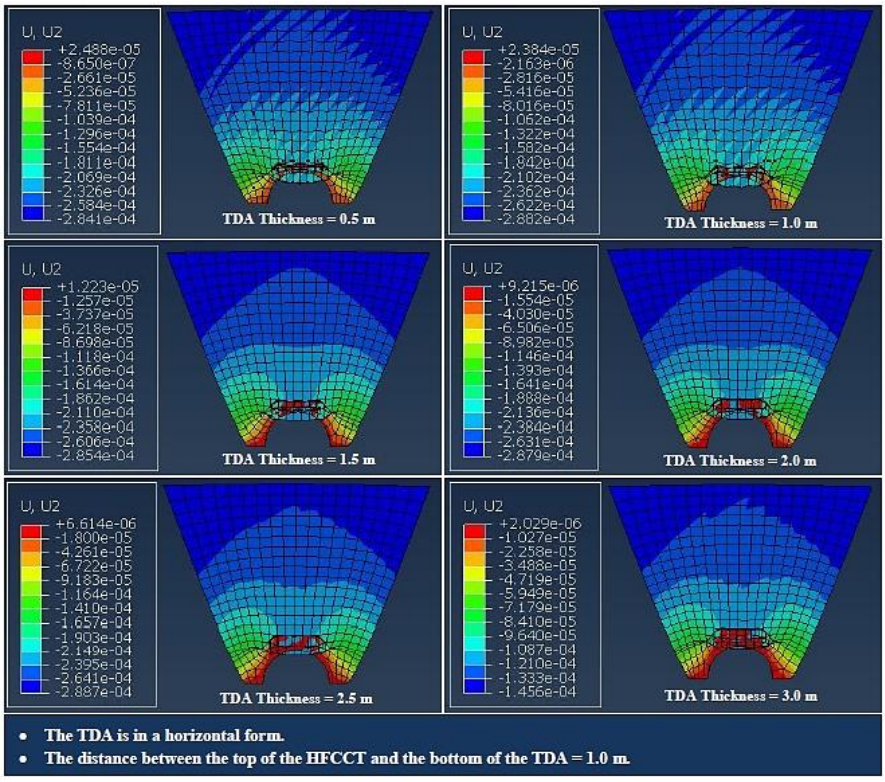

Figure 16: Contours of vertical displacement for using TDA with the thicknesses of 0.5 m, 1.0 m, 1.5 m, 2.0 m, 2.5 m, and 3.0 m in a horizontal form and the presence of geogrid on the top of the TDA and 1.0 m distance between the top of the HFCCT and the bottom of the TDA (as a method of load reduction on the HFCCT).

width deform in equal and uniform level. Meanwhile, the reduced VEP on the HFCCT structure is equal to the magnitude of the shear force on the soil in the interior prism. The VEP reduction will lead the LEP to be reduced as the LEP value mainly depends on γh (h: the height of backfill above the HCCT and γ: the unit weight of backfill material above the HCCT).

It is worth mentioning that the light gray color at the top of the interior prism in the backfill of the HFCCT in the contours of average LEP on the HFCCT with TDA inclusion in a combined horizontal and arch form with the presence of geogrid on top of the TDA refers to tensile forces resulting from the soil prism (interior prism) within the HFCCT structure width settle more than the surrounding soil prisms (exterior prisms) of the HFCCT backfill (see Figures 19, 20 and 21).

The idea of using the TDA in a combined horizontal and arch form was to reduce more VEP on the HFCCT by dissipating more VEP to the exterior soil prisms and then to the side slopes of the valley through increasing the soil arching effect that forms in the backfill of the HFCCT.

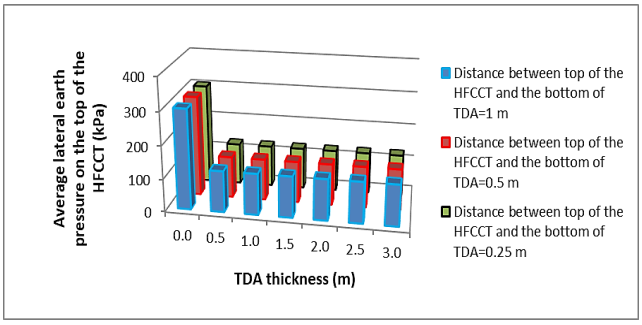

Figure 17: The relationship of the average LEP on top of the HFCCT study model with the TDA thickness (TDA is in a combined horizontal and arch form with the presence of geogrid on the top of the TDA) and the distance between the top of the HFCCT and the bottom of the TDA.

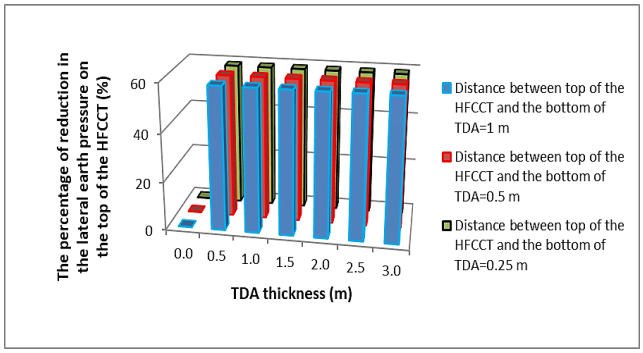

Figure 18: The relationship of the percentage of reduction in the LEP on top of the HFCCT study model with the TDA thickness (TDA is in a combined horizontal and arch form with the presence of geogrid on the top of the TDA) and the distance between the top of the HFCCT and the bottom of the TDA.

6. Conclusions

This study presents a numerical investigation of the coupled effect of using TDA as a compressible material and geogrid in two different forms on LEP reduction on HFCCTs. The research includes using tire-derived aggregate (TDA) and geogrid in horizontal and combined horizontal and arch forms above the HFCCT structure with six thicknesses; 0.5 m, 1.0 m, 1.5 m, 2.0 m, 2.5 m, and 3.0 m and three distances between the bottom of the TDA and top of the HFCCT; 0.25 m, 0.5 m, and 1.0m. The LEP reduction on HFCCTs occurs due to the relative vertical displacements of the HFCCT backfill soil prisms and soil arching. Several influential factors, including; the geogrid presence effect, the TDA form, the TDA thickness, and the distance between the top of the HFCCT and the bottom of the TDA were studied. Therefore, several conclusions can be drawn from this study:

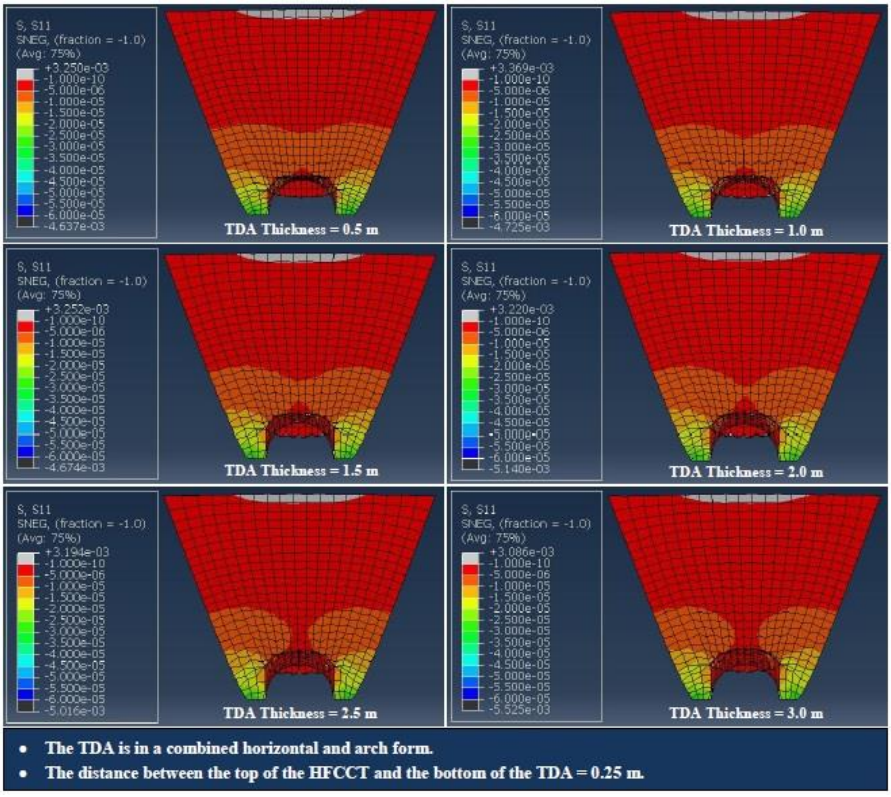

Figure 19: Contours of average LEP for using TDA with the thicknesses of 0.5 m, 1.0 m, 1.5 m, 2.0 m, 2.5 m, and 3.0 m in a combined horizontal and arch form and the presence of geogrid on the top of the TDA and 0.25 m distance between the top of the HFCCT and the bottom of the TDA (as a method of load reduction on the HFCCT).

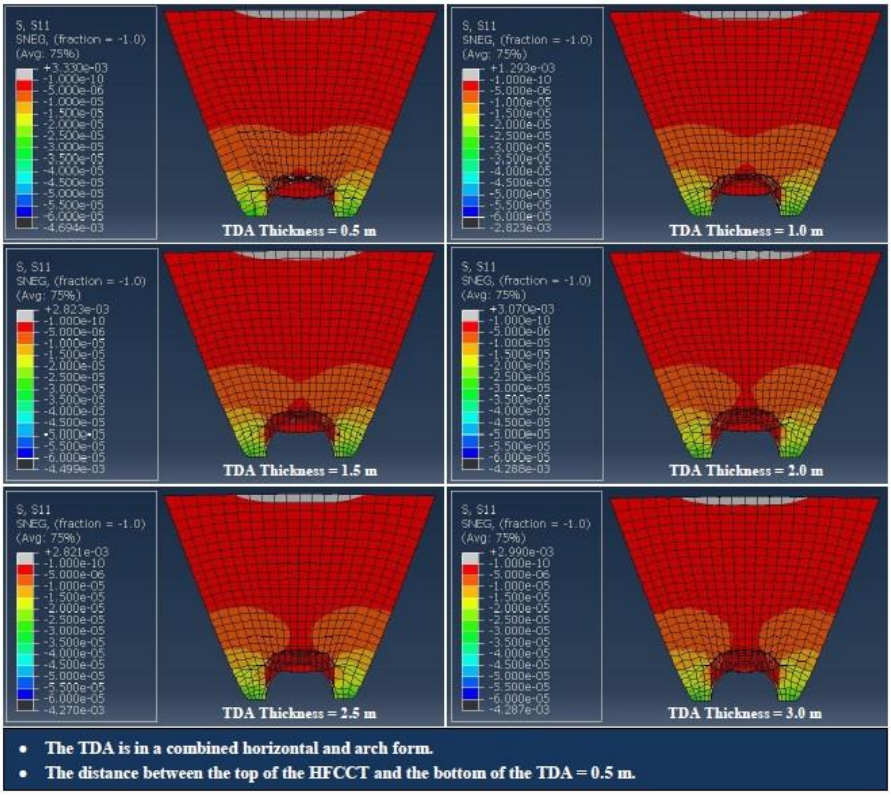

Figure 20: Contours of average LEP for using EPS TDA with the thicknesses of 0.5 m, 1.0 m, 1.5 m, 2.0 m, 2.5 m, and 3.0 m in a combined horizontal and arch form and the presence of geogrid on the top of the TDA and 0.5 m distance between the top of the HFCCT and the bottom of the TDA (as a method of load reduction on the HFCCT)

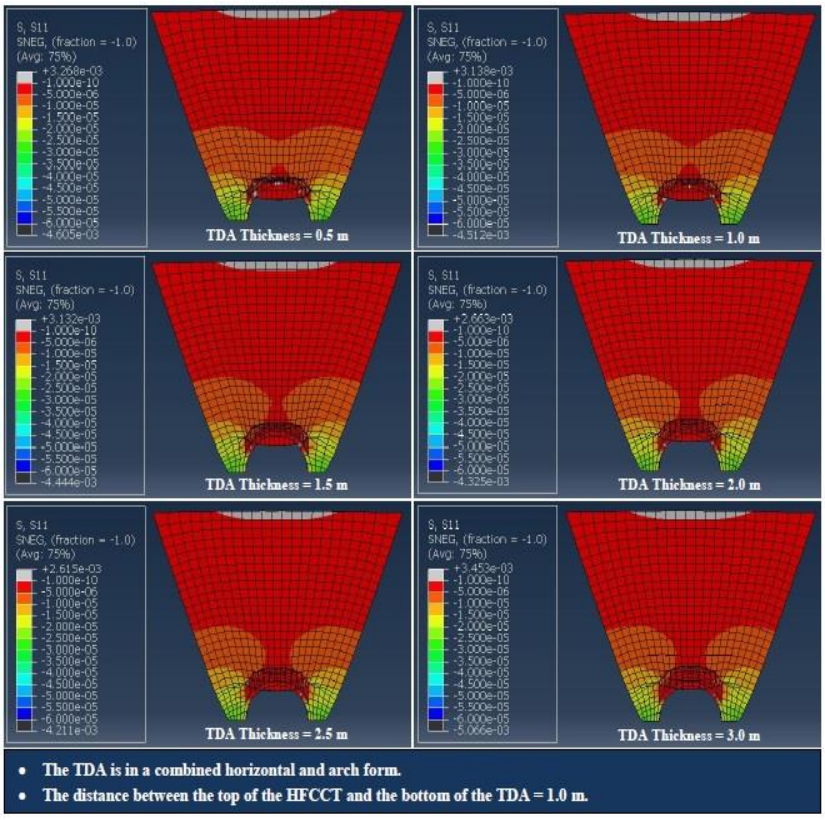

Figure 21: Contours of average LEP for using TDA with the thicknesses of 0.5 m, 1.0 m, 1.5 m, 2.0 m, 2.5 m, and 3.0 m in a combined horizontal and arch form and the presence of geogrid on the top of the TDA and 1.0 m distance between the top of the HFCCT and the bottom of the TDA (as a method of load reduction on the HFCCT).

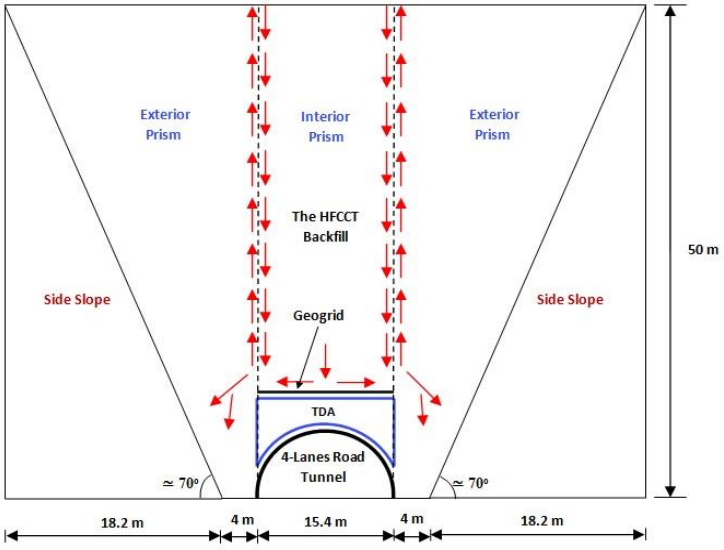

Figure 22: The effect of TDA inclusion in a combined horizontal and arch form with the presence of geogrid on the top of the TDA on the VEP reduction in the HFCCT study model.

1. Both forms of TDA and geogrid used in this study as methods of load reduction on the HFCCTs gave equal and good results in terms of average LEP reduction on the top of the HFCCT study model, where both TDA and geogrid forms resulted in 58.745% reduction in the average LEP on the top of the HFCCT study model.
2. For both forms of TDA and geogrid used in this study, and for all the TDA thicknesses and the distances between the bottom of the TDA and the top of the HFCCT study model, the average LEP on the top of the HFCCT study model reduced to the same value (125 kPa).
3. Although increasing the TDA thickness and the distance between the top of the HFCCT and the bottom of TDA in both methods of load reduction will not have any influence on the average LEP on the top of the HFCCT, they will have a considerable effect on the average LEP values in the other parts of the backfill of the HFCCT study model.
4. The presence of the TDA as a compressible material on the top of the HFCCT for load reduction purposes can help clean the environment by using large amounts of the scrap vehicles' tires in the form of TDA material.

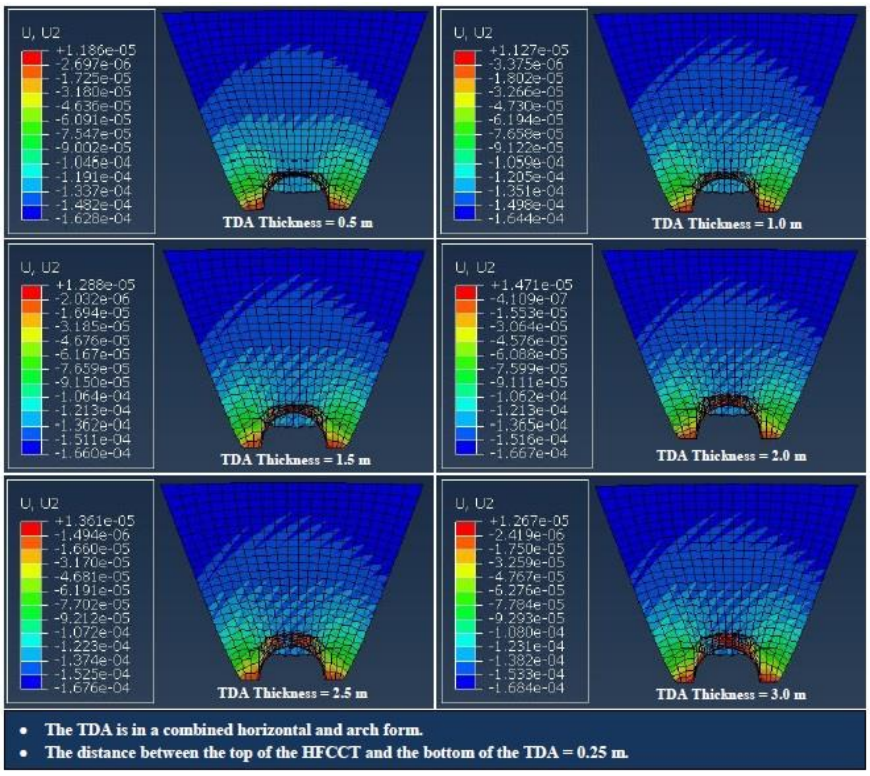

Figure 23: Contours of vertical displacement for using TDA with the thicknesses of 0.5 m, 1.0 m, 1.5 m, 2.0 m, 2.5 m, and 3.0 m in a combined horizontal and arch form and the presence of geogrid on the top of the TDA and 0.25 m distance between the top of the HFCCT and the bottom of the TDA (as a method of load reduction on the HFCCT).

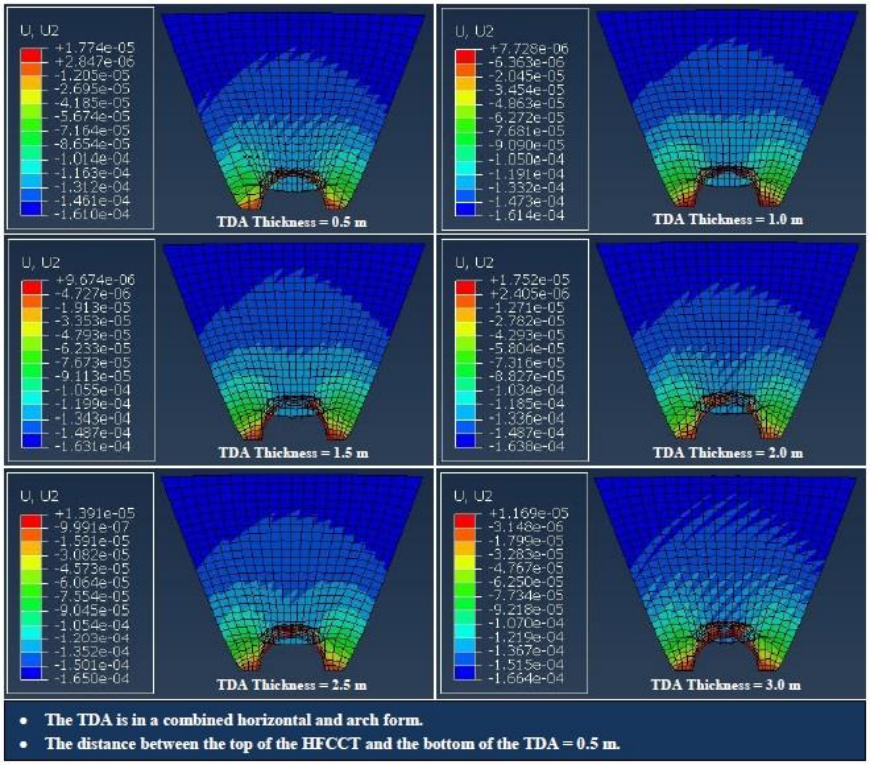

Figure 24: Contours of vertical displacement for using TDA with the thicknesses of 0.5 m, 1.0 m, 1.5 m, 2.0 m, 2.5 m, and 3.0 m in a combined horizontal and arch form and the presence of geogrid on the top of the TDA and 0.5 m distance between the top of the HFCCT and the bottom of the TDA (as a method of load reduction on the HFCCT).

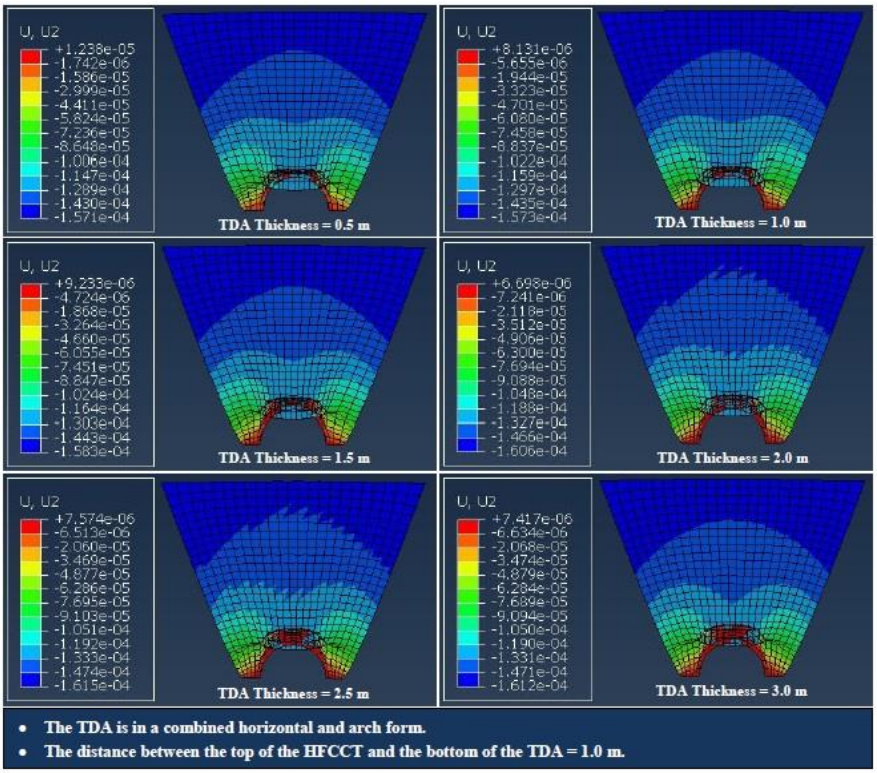

Figure 25: Contours of vertical displacement for using TDA with the thicknesses of 0.5 m, 1.0 m, 1.5 m, 2.0 m, 2.5 m, and 3.0 m in a combined horizontal and arch form and the presence of geogrid on the top of the TDA and 1.0 m distance between the top of the HFCCT and the bottom of the TDA (as a method of load reduction on the HFCCT).

Statements and Declarations

Competing Interests:

-The author received no direct or un-direct funding for this research.

-There is no conflict of interest.

REFERENCES

[1] S. Li, Y. Jianie, I.-H. Hom, L. Mam, Q. Wang, and B. Yu, "Experimental and Numerical Analyses for Earth Pressure Distribution on High-Filled Cut-and-Cover Tunnels," *KSCE J. Civ. Eng.*, 2020, doi: 10.1007/s12205-020-1693-7.

[2] M. G. Spangler, "A PRACTICAL APPLICATION OF THE IMPERFECT DITCH METHOD OF CONSTRUCTION A BRIEF DISCUSSION IS PRESENTED OF THE PRINCIPLES ON WHICH MARSTON ' S IMPERFECT DITCH METHOD IS BASED AND A," *Washington, DC Highw. Res. Board.*, vol. 37 of Proc, no. 37th Annual Meeting of the Highway Research Board, pp. 271–277, 1958.

[3] R. K. Taylor, "Induced-Trench Method of Culvert Installation.," *Highw Res. Rec.*, no. 443, pp. 15–31, 1973.

[4] J. A. Sladen and J. M. Oswell, "The induced trench method - a critical review and case history," *Can. Geotech. J.*, vol. 25, no. 3, pp. 541–549, 1988, doi: 10.1139/t88-059.

[5] J. Vaslestad, T. H. Johansen, and W. Holm, "Load reduction on rigid culverts beneath high fills: long-term behavior," *Transp. Res. Rec.*, no. 1415, pp. 58–68, 1993.

[6] A. Q. Gu, T. T. Guo, and X. P. Wang., "Experimental study on reducing load measurement using EPS of culvert under high-stacked soil," *Chinese J. Geotech. Eng.*, vol. 27, no. 5, p. 2005, 2005..

[7] R. P. McAffee and A. J. Valsangkar, "Field performance, centrifuge testing, and numerical modeling of an induced trench installation," *Can. Geotech. J.*, vol. 45, no. 1, pp. 85–101, 2008, doi: 10.1139/T07-086

[8] B. L. McGuigan and A. J. Valsangkar, "Centrifuge testing and numerical analysis of box culverts installed in induced trenches," *Can. Geotech. J.*, vol. 47, no. 2, pp. 147–163, 2010, doi: 10.1139/T09-085.

[9] S. Li, I. H. Ho, L. Ma, Y. Yao, and C. Wang, "Load reduction on high-filled cut-and-cover tunnel using discrete element method," *Comput. Geotech.*, vol. 114, no. March 2019, doi: 10.1016/j.compgeo.2019.103149.

[10] J. Kang, F. Parker, and C. H. Yoo, "Soil-Structure Interaction and Imperfect Trench Installations for Deeply Buried Concrete Pipes," *J. Geotech. Geoenvironmental Eng.*, vol. 133, no. 3, pp. 277–285, 2007, doi: 10.1061/(asce)1090-0241(2007)133:3(277).

[11] S. Li, G. Han, I.-H. Ho, L. Ma, Q. Wang, and B. Yu, "Coupled Effect of Cross-Sectional Shape and Load Reduction on High-Filled Cut-and-Cover Tunnels ConsideringSoil–Structure Interaction," *Int. J. Geomech.*, vol. 20, no. 7, p. 04020082, 2020, doi: 10.1061/(asce)gm.1943-5622.0001696.

[12] S. Li, Y. Yao, I.-H. Ho, L. Ma, Q. Wang, and C. Wang, "Coupled Effect of Expanded Polystyrene and Geogrid on Load Reduction for High-Filled Cut-and-Cover Tunnels Using the Discrete-Element Method," *Int. J. Geomech.*, vol. 20, no. 6, p. 04020052, 2020, doi: 10.1061/(asce)gm.1943-5622.0001683.

[13] S. Li, Y. Jianie, I.-H. Ho, L. Ma, B. Yu, and C. Wang, "Evolution of Load Reduction for High-Filled Cut-and-Cover Tunnels Subjected to Soil Creep," *Int. J. Geomech.*, vol. 21, no. 9, 2021, doi: 10.1061/(asce)gm.1943-5622.0002089.

[14] B. Yu, J. Xia, S. Li, and L. Zhao, "Optimization Effects of Load Reduction for Earth Pressure on High-Filled Cut-and-Cover

Tunnels Using the Discrete Element Method," *Adv. Civ. Eng.*, vol. 2021, 2021, doi: 10.1155/2021/8911818.

[15] L. M. Rodríguez, M. Arroyo, and M. M. Cano, "Use of tire-derived aggregate in tunnel cut-and-cover," *Can. Geotech. J.*, vol. 55, pp. 1–32, 2018, doi: https://doi.org/10.1139/cgj-2017-0446.

[16] ASTM-The American Society for Testing and Materials, "D 4253-00-Standard Test Methods for Maximum Index Density and Unit Weight of Soils Using a Vibratory Table1," West Conshohocken, PA 19428-2959, United States., 2000.

[17] Geosyntec Consultants, "Guidance Manual for Engineering Uses of Scrap Tires," 2008.

[18] D. Cheng, "Usage Guide-Tire-Derived Aggregate (TDA)," California State, 2016.

[19] F. H. Kulhawy and P. W. Mayne, "Manual on Estimating Soil Properties for Foundation Design," 1990.

[20] R. . Koerner, *Designing with Geosynthetics*, 5th ed. Pearson Prentice Hall, 2005.

[21] J. Han and D. Leshchinsky, "Geotextiles and Geomembranes Analysis of back-to-back mechanically stabilized earth walls," *Geotext. Geomembranes*, vol. 28, no. 3, pp. 262–267, 2010, doi: 10.1016/j.geotexmem.2009.09.012.

[22] Y. Dong, J. Han, and X. Bai, "Numerical analysis of tensile behavior of geogrids with rectangular and triangular apertures," *Geotext. Geomembranes*, vol. 29, 2010, doi: 10.1016/j.geotexmem.2010.10.007.

[23] C. H. Abdullah and T. B. Edil, "Behaviour of geogrid-reinforced load transfer platforms for an embankment on rammed aggregate piers," *Geosynth. Int.*, no. 3, 2007, doi: 10.1680/gein.2007.14.3.141.

[24] M. T. Adams and James G. Collin, "LARGE MODEL SPREAD FOOTING LOAD TESTS ON GEOSYNTHETIC," *J. Geotech. GEOENVIRONMENTAL Eng.*, no. January, pp. 66–72, 1997.

[25] S. F. Brown, J. Kwan, and N. H. Thom, "Identifying the key parameters that influence geogrid reinforcement of railway ballast," vol. 25, pp. 326–335, 2007, doi: 10.1016/j.geotexmem.2007.06.003.

[26] J. Han and K. Akins, "Use of Geogrid-Reinforced and Pile-Supported Earth Structures," *Deep Found.*, pp. 668–679, 2002.

[27] C. L. Helstrom, D. N. Humphrey, and S. A. Hayden, "Geogrid Reinforced Pavement Structure in a Cold Region," *Cold Reg. Eng.*, no. 401, pp. 1–12, 2006.

[28] J. Huang and J. Han, "Geotextiles and Geomembranes 3D coupled mechanical and hydraulic modeling of a geosynthetic-reinforced deep mixed column-supported embankment," *Geotext. Geomembranes*, vol. 27, no. 4, pp. 272–280, 2009, doi: 10.1016/j.geotexmem.2009.01.001.

[29] T. C. Kinney, K. S. Danielle, and J. Schuler, "Using Geogrids for Base Reinforcement as Measured by Falling Weight Deflectometer in Full-Scale Laboratory Study," *Transp. Res. Rec. 1611*, pp. 70–77, 1998.

[30] X. Tang, G. R. Chehab, and A. Palomino, "International Journal of Pavement Engineering Evaluation of geogrids for stabilizing weak pavement subgrade," *Int. J. Pavement Eng.*, vol. 9, no. 6, pp. 413–429, 2008, doi: 10.1080/10298430802279827.

[31] Y. Xiaoming, "An assessment of the geometry effect of geosynthetics for base course reinforcements," *Int. J. Transp. Sci. Technol.*, vol. 1, no. 3, pp. 247–257, 2012, doi: 10.1260/2046-0430.1.3.247.

[32] P. C. . ROUSÉ, "NUMERICAL MODELING AND ANALYSIS OF PULLOUT TESTS OF SHEET AND GEOGRID INCLUSIONS IN SAND," THE UNIVERSITY OF BRITISH COLUMBIA, 2018.

[33] W. Qingbiao *et al.*, "The Mechanical Property of Bidirectional Geogrid and its Application Research in Retaining Wall Design," *Open Constr. Build. Technol. J.*, pp. 214–222, 2015.

[34] A. Murashev, M. Easton, and P. Kathirgamanathan, "Advanced numerical modeling of geogrid-reinforced rockfall protection embankments Advanced Numerical Modelling of Geogrid-reinforced Rockfall Protection Embankments," *Proc. 19th NZGS Geotech. Symp.*, no. November 2013, 2013.

[35] K. Tharani, N. Mahendran, and T. J. Vijay, "Experimental Investigation of Geogrid Reinforced Concrete Slab," *Int. J. Eng. Adv. Technol.*, vol. 8, no. 3S, pp. 158–163, 2019.

[36] V. Vorobjovas and A. Vaitkus, "3D-FEM Analysis on Geogrid Reinforced Flexible Pavement Roads 3D-FEM Analysis on Geogrid Reinforced Flexible Pavement Roads," *Earth Environ. Sci.*, 2017, doi: doi :10.1088/1755-1315/95/2/022024.

[37] B. Sinmez, "Characterization of Geogrid Reinforced Ballast Behavior Through Finite Element Modeling," University of South Florida, 2019.

[38] M. Y. Abu-Farsakh, Q. Chen, and S. Yoon, "Use of Reinforced Soil Foundation (RSF) to Support Shallow Foundation," Louisiana, 2008.

[39] R. Zhou, Wan-huan; Lao, Jun-yuan; Huang, Yisheng; Chen, "Three-Dimensional Finite Element Modelling of Soil Arching in Pile-Supported Geogrid-Reinforced Embankments," *Procedia Eng.*, vol. 143, no. Ictg, pp. 607–614, 2016, doi: 10.1016/j.proeng.2016.06.081.

[40] A. H. Khodayari and R. Dabiri, "Effects of Geogrid Layers on Improving Bearing Capacity of Vibrating Machines Foundation," *J. New Approaches Civ. Eng.*, vol. 2, no. 2, pp. 11–26, 2018.

[41] M. Al-Barqawi, R. Aqel, M. Wayne, H. Titi, and R. Elhajjar, "Polymer geogrids: A review of material, design and structure relationships," *Materials (Basel).*, vol. 14, no. 16, 2021, doi: 10.3390/ma14164745.

[42] M. K. Fakhraldin, "MEASUREMENT OF TENSILE PROPERTIES OF GEOGRIDS Raid," *Second Int. Conf. Geotech. Constr. Mater. Environment*, 2012.